RSC Advances

ROYAL SOCIETY OF CHEMISTRY

www.rsc.org/advances

Uranium (VI) Adsorption from Aqueous Solutions Using Poly (vinyl alcohol)/ Carbon Nanotube Composites

Z. Abdeen[1], Z. F. Akl [2,*]

[1] Egyptian Petroleum Research Institute (EPRI), Petrochemicals department, P.O. Box 11727, Cairo, Egypt.

[2] Egyptian Nuclear and Radiological Regulatory Authority (ENRRA), Nuclear Safeguards and Physical Protection Department, P.O. Box 11762, Cairo, Egypt.

*Corresponding Author E-mail: eltasneem2007@yahoo.com , Tel:+(2)01065337270

Abstract

Poly (vinyl alcohol)/ multiwalled carbon nanotubes (PVA/MWCNTs) composite hydrogels were prepared by dispersion method and their ability to adsorb and remove uranyl ions from aqueous solutions was investigated. The prepared composites were characterized by XRD, TEM, SEM and FTIR. The effect of contact time, solution pH, initial UO_2^{2+} ions concentration and temperature on UO_2^{2+} ions adsorption from aqueous solution onto the prepared hydrogels was studied. The obtained results illustrated that, dispersion of MWCNTs into PVA matrix enhanced the removal efficiency of UO_2^{2+} ions compared to PVA only. The Langmuir and Freundlich adsorption models have been applied to evaluate the adsorption efficiency and the data were correlated well with Langmuir model. Thermodynamic parameters (ΔH°, ΔS°, ΔG°) were determined which indicated that UO_2^{2+} ions adsorption process onto the prepared hydrogels is exothermic and spontaneous. The adsorbed UO_2^{2+} can be desorbed effectively by 0.1 M EDTA.

***Keywords*:** Poly (vinyl alcohol); nanocomposites; uranyl ion; carbon nanotube, adsorption.

1. Introduction

Uranium is a radioactive element widely distributed over the earth's crust and it has a significant importance in nuclear industry since it is used as fuel for the nuclear power plants. In general, uranium released into the environment is often dissolved in aqueous solutions in the hexavalent form as UO_2^{2+}. Due to its strong radiation, uranium contamination can cause serious environmental problems [1]; therefore, uranium removal from aqueous solutions is important in view of nuclear fuel resources and human health [2]. In the last decades several techniques were developed for UO_2^{2+} ions removal from aqueous solutions. These techniques include precipitation, co-precipitation, solvent extraction, membrane dialysis, chromatographic

extraction, ion exchange, floatation and adsorption [3-8]. Among these techniques adsorption seems to be the most attractive one due to the advantages it has such as low cost, ease of operation, wide availability of adsorption materials and high resistance towards toxic chemical compounds in water [8]. Various kinds of new adsorbents for uranium removal and recovery have been reported [9-11], however, the adsorption capacity and selectivity of those adsorbents towards UO_2^{2+} ions need to be improved. Hydrophilic matrix adsorbents e.g. hydrogels as well as polymeric composites were also widely used to enhance the adsorption capacity of uranyl ions from aqueous solutions [12-13].

Nano-sized materials have attracted substantial interest in the scientific communities due to their unique physical and chemical properties such as large surface-to-volume ratio, high bioactivity, excellent conformation stability, good biocompatibity, excellent conductivity and catalytic efficiency [14]. Furthermore, nanoparticles surface atoms are unsaturated, and can, therefore, bind with other atoms that feature high chemical activity. In recent years, various kind of nano-sized materials have been prepared [15] and found potential applications in many fields such as photocatalysis [16], optical sensors [17] and medical applications [18]. Nanomaterials including traditional inorganic nanoadsorbents and novel polymer supported composites have been extensively applied for pollutants removal from aqueous solutions, due to their novel size- and shape-dependent properties, contributing to their excellent removal efficiency [19-20].

Multiwalled carbon nanotubes (MWCNTs) have inherent extraordinary structural, mechanical, thermal and electronic properties which made them attractive in the field of radionuclide adsorption [21]. Polymeric/MWCNTs nanocomposites have been applied extensively in uranium adsorption due to their highly porous and hollow structure, large specific surface area and light mass density [22-23]. However, problems associated with the dispersion of MWCNTs fillers and load transfer across the polymer-CNTs interface may limit polymer/CNTs composites usage. Therefore, it is of great significance to improve the dispersion of MWCNTs into the polymeric composites. Many efforts have been made to overcome these barriers including using of surfactants [24], high shear mixing [25], chemical modification [26] and in-situ polymerization [27].

Poly (vinyl alcohol) (PVA) is a water-soluble, cheap, nontoxic, hydrophilic, biocompatible synthetic polymer containing large amounts of hydroxyl groups [28]. PVA has excellent film

forming, emulsifying and adhesive properties, high tensile strength and good flexibility. PVA blending with other polymers and fillers widens its range of applications [29]. Further improvement of PVA properties was achieved by synthesis of PVA/MWCNTs nanocomposites [30-31]. It was reported that PVA/CNTs composites have a wide range of applications, from biomedical to electromechanical [32] and their properties depend on the attributes and dispersion of MWCNTs [33]. PVA is a promising candidate in UO_2^{2+} ions removal, because of its high degree of swelling in water, high durability and chemical stability [34-35].

The purposes of the current study are: (1) to present a simple and environmental friendly method for preparation of MWCNTs/PVA nanocomposites; (2) to improve the dispersion of MWCNTs in PVA matrix through sodium dodecyl sulphate treatment; (3) to characterize prepared MWCNTs/PVA nanocomposites by X-ray diffraction (XRD), scanning electron microscopy (SEM) and fourier transform infrared (FTIR) spectroscopy; and (4) to investigate the feasibility of UO_2^{2+} ions adsorption by the prepared composites under different experimental conditions.

2. Experimental

2.1. Materials

PVA with average $M_{w,}$ 127,000 and the degree of hydrolysis 89%, was purchased from Merck, (Germany). Epichlorhydrin (E), potassium hydroxide, sodium dodecyl sulphate (SDS) and other chemicals were obtained from Beijing chemical reagent factory (China) and used without further purification. MWCNTs were supplied from the Egyptian Petroleum Research Institute. According to the product specification, the as-grown MWCNTs have an average particle size of 20-30 nm and purity above 97%. Oxidized MWCNTs were prepared by oxidization with a mixture of concentrated nitric acid and sulfuric acid (1:3, V/V) [36]. The surface area of MWCNTs was determined using N_2-BET method (micromeritics Surface Area and Porosity Analyzer, ASAP 2020, American) and was found to be 99 m^2/g. UO_2^{2+} stock solution was prepared by dissolving significant amount of $[UO_2(NO_3)_2 \cdot 6H_2O]$, supplied by Mallinckrodt Company, in deionized water.

2.2. Preparation of PVA/CNTs/E and PVA/CNTs/SDS/E composite hydrogels

The synthesis procedure for a typical PVA/MWCNTs nanocomposite (3.0 wt %) was as the following: MWCNTs powder (30 mg) was dispersed in distilled water (15 mL) in an ultrasonic

bath (Branson 2510) for 60 min at room temperature. Subsequently, an aqueous solution (10 mL) of PVA (1.0 g) was added to the MWCNTs suspension. Sonication was continued for an extra 60 min to yield a stable black-colored suspension. Afterwards, stoichiometric amounts of the crosslinker (epichlorohydrin) and potassium hydroxide solution were added separately to the suspension with additional sonication for 30 min at room temperature [37]. Finally, this homogeneous PVA/CNTs/E mixture was poured into a Teflon Petri dish and kept at 50°C for film formation until its weight reached an equilibrium value. This previous procedure was repeated but in absence the MWCNTs to produce PVA/E film.

PVA/CNTs/SDS/E composite hydrogel was prepared by mixing MWCNTs powder with SDS solution (30 wt%) (MWCNTs:SDS = 1:10) and sonication gently at room temperature for 5 hours to form a stable aqueous dispersion of MWCNTs which was kept at room temperature for 72 hours, then the abovementioned procedure was repeated to produce PVA/CNTs/SDS/E film.

2.3. Structural analysis

Chemical structures of the prepared hydrogels were analyzed by FTIR system (Shimadzu 8001, Japan). Morphological evaluations of the prepared hydrogels before and after UO_2^{2+} ions adsorption were made using SEM (JEOL, 6510 LA, Japan). Transmission electron microscope TEM images of the prepared nanocomposites were obtained using TEM (JEOL, JEM-2100, Japan) at an accelerating voltage of 200 kV, after samples ultrasonication in deionized water for 20 min and dispersion on copper grids. XRD (PANalytical, X'pert PRO, Germany) was used to investigate the structure of the prepared nanocomposites. The XRD measurements were carried out in the 2θ angle with the range of 5-70°. Energy-Dispersive X-ray Spectrometer (EDX) (JEOL, 6510 LA) was used to confirm UO_2^{2+} ions adsorption by detecting U lines.

2.4. Swelling behavior of the prepared hydrogels

A known weight of the sample disc was immersed in solutions of different pHs (3, 5 and 7) at 30 ^{0}C until the swelling equilibrium was reached. The disc was removed, dried with absorbent paper to get rid of excess water then weighed. The degrees of swelling (DS) for the prepared hydrogels were calculated at different time intervals using the following equation:

$$DS = \frac{m - m'}{m'} \qquad (1)$$

where m and m' denote the weights of hydrogel and dried hydrogel sample, respectively [38].

2.5. Uranyl ions adsorption studies

Adsorption of UO_2^{2+} ions from aqueous solutions onto the prepared hydrogels was investigated in a batch-wise method. Aqueous solutions (50 mL) containing different amounts of UO_2^{2+} ions were incubated with the hydrogels (0.03 g) at different initial pHs, (adjusted with 0.1 mol/L HNO_3 and 0.1 mol/L NaOH) and allowed to equilibrate for different conditions while being shaken continuously. Aqueous solutions were separated from the hydrogels at desired intervals and the residual concentrations of UO_2^{2+} ions were determined by the Arsenazo-III spectrophotometric method using UV-Visible spectrophotometer (Thermo Evolution 300, England). The amount of UO_2^{2+} ions adsorbed per unit mass of the hydrogels was calculated using the following expression:

$$q_e = \frac{(C_o - C_e)\,V}{W} \qquad (2)$$

where, q_e is the adsorption capacity of the hydrogels (mg/g); C_o and C_e are the concentrations of UO_2^{2+} ions in the initial and equilibrium solution (mg/L), respectively, V is the volume of the aqueous solution (L) and W is the mass of dry hydrogels (g).

To investigate the desorption ability of adsorbed UO_2^{2+} from PVA/MWCNTs nanocomposites, desorption experiments were carried using 0.1 M HNO_3, H_2SO_4 and EDTA. After the adsorption reached equilibrium, PVA/MWCNTs composites loaded with UO_2^{2+} ions were separated, washed, dried, added to 25 ml of the desired eluent for desorption and shacked at 150 rpm for 4 h. After that the adsorbent was separated washed and dried for the successive adsorption–desorption cycles.

The difficulty in preparing well dispersed MWCNTs composite solutions resulted from their high specific surface area which resulted in very strong van der Waals interactions. Surfactants are widely used to disperse MWCNTs uniformly without breakage and aggregation. It was reported that, using SDS in the preparation of PVA/CNTs composites resulted in good nanotube dispersion and load transfer from polymer matrix to the carbon nanotubes and consequently improve the composites properties [23].

Experimental work using uranyl nitrate hexahydrate was carried out in the safeguards destructive analysis laboratory (KMP-I) at the Egyptian Nuclear and Radiological Regulatory Authority (ENRRA).

3. Results and discussion

3.1. Structural evaluation

FTIR spectra of the prepared MWCNTs powder, PVA/E, PVA/CNTs/E and PVA/CNTs/SDS/E were recorded and shown in Figure 1. Peaks at 1000-1300 cm^{-1} attributed to the absorption of stretching vibration of C-O bonds. The other peaks at 1616 and 1386 cm^{-1} can be assigned to the nitro groups on the surface of carbon materials, as a result of the efficiency of the modification with nitric acid that was demonstrated by a significant increase in the C–O and –NO functional groups. Peaks at 2921-2930 cm^{-1} are correlated to C–H. Peaks at 3230–3330 cm^{-1} are assigned to –OH stretching vibration. The intramolecular and intermolecular hydrogen bonds of the OH groups of PVA and other molecule shifted the band of –OH group to lower frequencies as shown in the PVA spectra. It is noted that there is no characteristic change observed in the peaks around the wavelength range of 3200–3600 cm^{-1} for PVA/CNTs/E and PVA/CNTs/SDS/E composite hydrogels, suggesting that the dispersion of the incorporated CNTs within the film was essentially physical and the basic chemical characteristic of the prepared material remained intact after their incorporation. Peaks observed at 1221 and 1146 $cm^{-1}$of PVA/CNTs/SDS/E spectra are assigned to sulfate groups of SDS. Peak at 1060 cm^{-1} in all spectra is for (C–O–C) as a result of formation of crosslinked network structures. The peak around 1095 cm^{-1} denotes C-O stretching of the secondary alcoholic groups [37, 28].

The XRD profiles of MWCNTs powder, PVA/E, PVA/CNTs/E and PVA/CNTs/SDS/E samples were represented in Figure 2. The characteristic diffraction peak of CNTs appeared clearly at $2\theta = 26.2°$, implying that its d-spacing resembles the one of pristine graphite. Whereas, the diffraction peaks of PVA/E film are found at 18.7° (main), as well as 9.7, 20.1 and 29.7° (minor) [39]. The XRD pattern of the PVA/CNTs/E composite film has some peaks which were assigned to CNTs and PVA/E. This means that CNTs sheets were not individually dispersed in PVA matrix but rather in the form of few-layer CNTs platelets. In addition, PVA/E composite film shows an amorphous peak at 19.4°, however CNTs sheets shows a peak of diminished intensity at 23.4°. This result indicates that CNTs had been efficiently exfoliated within the PVA matrix. The crystalline structure of CNTs may be as a result of CNTs overload which is not intercalated into the PVA matrix. On the other hand, PVA/CNTs/SDS/E composite shows the exfoliated peak for PVA composite film and a weak peak for CNTs. This revealed that CNTs were well exfoliated due to its homogenous dispersion in PVA matrix by adding SDS [39].

3.2. Water content

The swelling behavior of prepared hydrogels at different time intervals was investigated and illustrated in Figure 3. The water affinity of the pure hydrogel (PVA/E) may be attributed to the PVA hydroxyl group, since this hydrophilic group is capable of forming hydrogen bond with water molecules [39]. The hydrogel containing SDS relatively swelled in a higher degree compared to PVA/CNTs/E and PVA/E hyrogels. This may be due the fact that, the hydrophobic backbone of SDS interacts with MWCNTs though hydrophobic interaction and thereby anchors the SDS molecules onto the surface of MWCNTs, leaving the hydrophilic head groups to interact with the polymer [40], resulting in increasing the possibility of water uptake into the film and enhancement of the swelling behavior.

3.3. Microscopic investigations

The surface morphology of the prepared hydrogels, before and after UO_2^{2+} ions adsorption, was investigated using SEM and represented in Figure 4. It is clear from SEM images that there is an obvious change in PVA morphology by introduction of CNTs and the morphology of PVA/CNTs resembles a hybrid composition of its components, while the dark colored textural appearances on PVA after CNTs inclusion are due to the impression of CNTs crystallites. Eventual consequence of IR, XRD and SEM reveals the homogeneous formation of the composites and uniform dispersion of MWCNTs in PVA network. It can be observed from Figure 4 that, all composites are porous; and have rough surface especially for composites containing CNTs and SDS. It can be also observed that, pores size or pores-content has considerably increased in all samples after UO_2^{2+} ions adsorption. Uranium adsorption process results in some destruction of the hydrogels ordered structure which may be attributed to the electrostatic repulsion of the partially protonated adsorption sites of the hydrogels with the positively charged UO_2^{2+} ions [41].

Figure 5 shows the characteristic TEM image of MWCNTs. This micrograph shows that CNTs have smooth surface and integrated hollow tubular structure and most of the impurity phases, such as amorphous carbon and graphitic nanoparticles, were removed. The diameter of the MWNTs was 20-30 nm.

3.4. Uranium adsorption studies

3.4.1. Effect of pH

pH of the aqueous solution is an important parameter that influences metal ion speciation and total surface charge on the chelating resin. The pH effect on UO_2^{2+} ions adsorption onto the prepared nanocomposites was investigated for the pH range of 1.0-5.0 at 25°C. The adsorption capacity as a function of equilibrium pH was illustrated in Figure 6. It can be seen from Figure 6 that UO_2^{2+} ions adsorption capacity depends on the solution pH value, as the adsorption efficiency increases with pH increasing to a maximum value (pH 3.0) and then decreases with further increase in the solution pH. The maximum adsorption at pH 3 may be due to the formation of U(VI) complexes with carboxyl groups on the surface of MWCNTs and PVA alcoholic groups. At low pH condition (pH < 3.0), the main effective adsorption sites of the hydrogels are easily protonated leading to the reduction of the adsorptive activity [42]. However, the availability of free uranium (VI) ions is maximum at pH 3.0 and hence maximum adsorption is obtained [43]. With further increase in the solution pH, hydrolysis precipitation starts due to the formation of complexes in aqueous solution. Hydrolysis products such as $UO_2(OH)^+$, $UO_2(OH)_2^{2+}$ and $(UO_2)_3(OH)_5^+$ are formed [44] which results in decline of adsorption efficiency of uranium (VI).

3.4.2. Effect of contact time

To understand the effect of contact time on UO_2^{2+} ions adsorption onto the prepared nanocomposites, adsorption experiments were conducted for contact times ranging from 1 to 200 minute and the obtained results were represented in Figure 7. The results revealed that UO_2^{2+} ions adsorption kinetics had two stages: an initial fast stage where adsorption was fast and contributed significantly to equilibrium uptake, and a slower second phase whose contribution to the total UO_2^{2+} ions adsorption was relatively small. The change in the rate of UO_2^{2+} ions adsorption might be due to the fact that initially all adsorbent sites were vacant and the solute concentration gradient is high. Afterwards, UO_2^{2+} ions adsorption rate decreased significantly due to the decrease in adsorption sites. The quick adsorption of UO_2^{2+} ions suggests that chemical adsorption rather than physical adsorption contributes mainly to the UO_2^{2+} ions adsorption [45].

3.4.3. Effect of initial concentration

The effect of UO_2^{2+} ions initial concentration on the adsorption efficiency was studied by contacting a fixed mass of the prepared nanocomposites at a fixed temperature (25°C) and pH

(3.0) using a range of initial UO_2^{2+} ions concentrations (100, 200, 300, 500, 700, and 1000 mg/L). The adsorption data at different initial UO_2^{2+} ions concentrations was shown in Figure 8**.** It can be seen that, the adsorption capacities increase with the increment of UO_2^{2+} ions initial concentration. This may be due the fact that, the initial concentration provides the driving force to overcome the resistance to the mass transfer of UO_2^{2+} ions between adsorbent and adsorbate [46]. Meanwhile, the initial concentration was high and then the driving force was high too, and therefore the adsorption capacity would be high.

3.4.4. Evaluation of adsorption isotherm models

In order to understand the adsorption behavior the prepared nanocomposites for UO_2^{2+} ions, the equilibrium data were evaluated according to the Langmuir and Freundlich isotherms models under the experimental conditions.

Langmuir isotherm model assumes that the adsorbent surface is homogeneous and the adsorption sites are energetically identical indicating that the adsorbed molecules don't react with each other. The linear form of Langmuir equation can be depicted as [47]:

$$\frac{C_e}{q_e} = \frac{C_e}{Q} + \frac{1}{Q_{max}b} \qquad (3)$$

where q_e (mg/g) represents the amount of solute adsorbed per unit weight of adsorbent at equilibrium; C_e (mg/L) is the equilibrium solute concentration in solution, Q_{max} (mg/g) is the maximum monolayer adsorption and b (L/mg) the Langmuir constant related to the affinity of binding sites.

The linear form of Freundlich isotherm can be expressed as [48]:

$$\log q_e = \log k_F + \frac{1}{n}\log C_e \qquad (4)$$

where k_F and n are the Freundlich constants, which represent adsorption capacity and intensity, respectively.

Langmuir and Freundlich sorption isotherms of UO_2^{2+} ions on the surface of the prepared hydrogels were elaborated in Figures 9A and 9B respectively, and the relative coefficients obtained from fitting isotherm patterns were listed in Table 1 Parameter values for two kinds of models are presented in Table 1. As indicated from the correlation coefficients in Table 1, Langmuir model fits better than Freundlich model for UO_2^{2+} ions adsorption on the prepared

nanocomposites (correlation coefficient is 0.99). This result suggests that the prepared nanocomposite surface has similar adsorption performance and thus the adsorbed UO_2^{2+} ions do not compete with each other and are adsorbed by forming nearly complete monolayer coverage of the nanocomposite particles. This phenomenon suggests that chemo-sorption is the primary adsorption mechanism in adsorption reaction [49]. The obtained values of the Langmuir equation parameters specify a high enough adsorption activity of the synthesized sorbent towards uranyl ions [50].

Based on the Langmuir equation, Q_{max} values of UO_2^{2+} onto PVA/E, PVA/CNTs/E and PVA/CNTs/SDS/E were 121.95, 172.41 and 232.55 mg/g respectively, indicating that the adsorption capacity of the prepared nanocomposite has the following order PVA/E<PVA/CNTs/E<PVA/CNTs/SDS/E. This can be explained as the following: adding MWCNTs to PVA increases the functional groups in the composites consequently the adsorption capacity will increase. It was reported that oxidation of carbon surface can offer not only more hydrophilic surface structure, but also a large number of oxygen-containing functional groups like –COOH, –OH, or –C=O on the surfaces of MWCNTs, which increase the adsorption capability of carbon material [51]. The presence of the ionic surfactant, SDS, decreases MWCNTs aggregative tendency in water and enhance their dispersion via noncovalent approach, and therefore enhance the adsorption [52].

3.5. Adsorption thermodynamics

Thermodynamic parameters including enthalpy change (ΔH°), Gibbs free energy change (ΔG°) and entropy change (ΔS°) were estimated by using equilibrium constants changing with temperature. For this purpose temperature effect on UO_2^{2+} ions adsorption was investigated using a water bath with a fixed amount of the prepared nanocomposites at pH 3, and contact time of 180 min for three temperatures: 303, 313 and 323 K. Thermodynamic parameters (ΔH° and $\Delta S\circ$) for uranium adsorption on the prepared nanocomposites were calculated from the linear plot of $\ln K_d$ Vs 1/T (Figure 10), using the following relations [52]:

$$K_d = \frac{amount\ of\ metal\ in\ adsorbent}{amount\ of\ metal\ in\ solution} \cdot \frac{V}{M} \qquad (5)$$

$$\ln K_d = \frac{\Delta S^o}{R} - \frac{\Delta H^o}{RT} \qquad (6)$$

where K_d is the distribution coefficient (mL/g), ΔS° is standard entropy, ΔH° is standard enthalpy, T is the absolute temperature (K) and R is the gas constant (J mol^{-1} K^{-1}).

The standard free energy values were calculated from the following equation:

$$\Delta G^o = T\Delta H^o - \Delta S^o \qquad (7)$$

Thermodynamic parameters for UO_2^{2+} ions adsorption onto the prepared nanocomposites were listed in Table 2. Negative values of ΔH° and the decrease in the value of ΔG° with rise in temperature reveal that the adsorption of UO_2^{2+} ions on the prepared nanocomposites is exothermic process in nature and favored at low temperature. Negative free energy values ΔG° indicates the feasibility of the process and its spontaneous nature. Positive values of ΔS° reflect the affinity of the prepared nanocomposites toward UO_2^{2+} ions in aqueous solutions and suggest the increased randomness at the solid-solution interface during adsorption [53].

3.6. Desorption analysis

The stability and potential regeneration of the prepared nanocomposites were investigated through desorption. Adsorption/desorption of UO_2^{2+} ions onto nanocomposites was studied in a batch mode using H_2SO_4, HNO_3 and EDTA as eluents and the results were represented in Figure 11. The results indicate that UO_2^{2+} ions can be desorbed efficiently by 0.1 mol/L EDTA solution. As can be seen from Figure 11, the adsorption capacity of PVA/MWCNTs nanocomposites towards UO_2^{2+} ions decreases slightly from 98.5 to 92.0% after third cycle.

4. Conclusions

PVA/MWCNTs nanocomposites have been prepared as simple, efficient and feasible UO_2^{2+} ions adsorbents. The prepared nanocomposites were characterized by XRD, SEM, TEM and FTIR to determine their chemical constituents, micro-structures and functional groups. UO_2^{2+} ions uptake experiments have been carried out by the batch method and the conditions have been optimized. The obtained results show the high adsorption capacity towards UO_2^{2+} ions as 121.95, 172.41 and 232.55 mg/g for PVA/E, PVA/CNTs/E and PVA/CNTs/SDS/E, respectively. The thermodynamic parameters ΔH°, ΔS° and ΔG° values of UO_2^{2+} ions adsorption onto the prepared nanocomposites show the process is exothermic and spontaneous in nature. In conclusion, we succeeded to impart the excellent properties of MWCNTs to PVA matrix and to prepare nanocomposite hydrogels which can be used effectively to remove UO_2^{2+} ions from aqueous solutions.

References

[1] E. Craft, A. Abu-Qare, M. Flaherty, M. Garofolo, H. Rincavage and M. Abou-Donia, *J. Toxicol. Environ. Health B Crit. Rev.* 2004**, 7,** 297-317.

[2] S.C. Sheppard, M. I. Sheppard, M.O. Gallerand and B. Sanipelli, *J. Environ. Radioact.* 2005, **79,** 55-83.

[3] J.L. Lapka, A. Paulenova, M.Y. Alyapyshev, V.A. Babain, R.S. Herbst and J.D. Law, *Radiochim. Acta*, 2009, **97**, 291-296.

[4] D.E. Crean, F.R. Livens, Mustafa Sajih Martin C. Stennett, Daniel Grolimund, C.N. Borcac and N.C. Hyatt, *J. Hazard. Mater.*, 2013, **263,** 382-390.

[5] Lucy Mar Camacho, Shuguang Deng and Ramona R. Parra, *J. Hazard. Mater*., 2010, **175,** 393-398.

[6] S. B. Xie, C. Zhang, X. H. Zhou, J. Yang, X.J. Zhang and J.S. Wang, *J. Environ. Radioactiv.,* 2009, **100**, 162-166.

[7] A. M. Atta, Z. H. Abd El Wahab, Z. A. El Shafey, W. I. Zidan and Z F. Akl, *J. Dispersion Sci. Technol.,* 2010, **31,** 1601-1610.

[8] S. Zhang, M. Zeng, J. Li, J. Li, J. Xu and X. Wang, *J. Mater. Chem. A,* 2014, **2**, 4391-4397.

[9] A. Gajowiak, M. Majdan and K. Drozdzal*, Przem. Chem*., 2009, **88,** 190-196.

[10] I. Zhuravlev, O. Zakutevsky, T. Psareva, V. Kanibolotsky, V. Strelko, M. Taffet and G. Gallios, *J. Radioanal. Nucl. Chem.,* 2002, **254,** 85-89.

[11] K. Oshita, M. Oshima, Y.H. Gao, K.H. Lee and S. Motomizu, *Anal. Chim. Acta,* 2003, **480,** 239-249.

[12] Y. Zhao, J. Li, S. Zhang, H. Chen and D. Shao, *RSC Adv***.**, 2013, **3**, 18952-18959.

[13] Y. Liu, Qin Li, X. Cao , Y. Wang, X. Jiang, M. Lee, M. Hua and Z. Zhang, *Appl. Surf. Sci*., 2013, **285**, 258-266.

14. P. Liang, Y.C. Qin, B. Hu, T.Y. Peng and Z.C. Jiang*, Anal. Chim. Acta,* 2001, **440**, 207-213.

[15] S. Zhang, J. Li, X. Wang, Y. Huang, M. Zeng and J. Xu, *J. Mater. Chem. A*, 2015, 3, 10119–10126.

[16] S. Zhang, J. Li, X. Wang, Y. Huang, M. Zeng and J. Xu, *J. ACS Appl. Mater. Interfaces,* 2014, **6**, 22116-22125.

[17] M. Cui, J. Huang, Y. Wang, Y. Wu and X. Luo, *Biosens. Bioelectron.,* 2015, **68,** 563-569.

[18] S. Prabhu and E. K Poulose, *Int. Nano Lett*., 2012, **2**, 32-33.

[19] S. Zhang, J. Li, X. Wang, Y. Huang, M. Zeng and J. Xu, *J. Mater. Chem. A,* 2013, **1**, 11691-11697.

[20] X. Wang, Y. Guo, L. Yang, M. Han, J. Zhao and X. Cheng*, J. Environ. Anal. Toxicol.,* 2012, **2**,154-161.

[21] J. Wang, P. Liu, Z. Li, W. Qi, Y. Lu and W. Wu, *Materials,* 2013, **6**, 4168-4185.

[22] A. Gopalan, M. F. Philips, J. H. Jeong and K. P. Lee, *J.* Nanosci, *Nanotechnol.*, 2014, **14,** 2451-2458.

[23] J. N. Dawoud, *Appl. Surf. Sci*., 2012, **259**, 433-440.

[24] V. V. Didenko, V.C. Moore, D.S. Baskin and R.E. Smalley, *Nano Letters*, 2005, **5,** 1563-1567.

[25] R. B. Mathur, S. Seth, C. Lal, R. Rao, B. P. Singh and T. L. Dhami, *Carbon*, 2007, **45,**132-40.

[26] Zhe Wang, H. A. Colorad, Zhan-Hu Guo, Hansang Kim, Cho-Long Park, H. Tomas Hahn, Sang-Gi Lee, Kun-Hong Lee and Yu-Qin, *Mat. Res.*, 2012, **15,** 510-516.

[27] B. S. Stankovich, D. A. Dikin, R. D. Piner, K. A. Kohlhaas, A. Kleinhammes, Y. Jia, Yue Wu, S. T. Nguyen and S. Rodney, *Carbon*, 2007, **45,** 1558-1565.

[28] Z. Abdeen, *J. Dispersion Sci. Technol.,* 2011, **32,** 1337-1344.

[29] J. Jose1, S. K. De1, M. Al-Ali, J. B. Dakua, P. A Sreekumar, R. Sougrat and M. A. Al-Harthi, *Starch*, 2015, **67***,* 147-153**.**

[30] P. Zhang, T. Zhou, L. He, S. J. Sun, J. Wang, C. Qin and L. Dai, *RSC Adv.***,** 2015, **5**, 55492-55498.

[31] P. Zhang, D. Qiu, H. Chen, J. Sun, J. Wang, C. Qin and L. Dai, *J. Mater. Chem. A***,** 2015, **3**, 1442-1449.

[32] C. W. Lou, Z. I. Lin, C. L. Huang, W. C. Chen, C. K. Chen and J. H. Lin, *Appl. Mech. Mater.,* 2015, **749**, 182-185.

[33] Fei-Peng Du, En-Zhou Ye, Wen Yang, Tian-Han Shen, Chak-Yin Tang, Xiao-Lin Xie, Xing-Ping Zhou and Wing-Cheung Law, *Composites Part B*, 2015, **68**, 170-175.

[34] F. T. Chi, S. Hu, J. Xiong and X. Wang, *journal of Sci. China Chem.*, 2013, **56,** 1495-1503.

[35] Y. Liu, X. Caoc, R. Huac, Y. Wang, Y. Liu, C. Pang and Y. Wang, *Hydrometallurgy*, 2010, **104,** 150-155.

[36] S. T. Yang, W. Guo, Y. Lin, X. Y. Deng, H. F. Wang, H. F. Sun, Y. F. Liu, X. Wang, W. Wang, M. Chen, Y. P. Huang and Y. P. Sun, *J. Phys. Chem. C*, 2007, **111**, 17761-17764.

[37] A.M. AL-Sabagh and Z. Abdeen, *J. Polym. Environ*., 2010, **18,** 576-583.

[38] L. Liu, A. H. Barber, S. Nuriel, and H. D. Wanger, *Adv. Funct. Mater.*, 2005, **15**, 975-980.

[39] J. Liang, Y. Huang, L. Zhang, Y. Wang, Y. Ma, T. Guo and Y. Chen, *Adv. Funct. Mater.,* 2009, **19,** 2297-2302.

[40] Y. Kim, N. Minami and S. Kazaoui, *Appl. Phys Lett*., 2005, **86,** 073103-1-073103-3.

[41] M. Kokabi, M. Sirousazar and Z. M. Hassan, *Eur. Polym. J.,* 2007, **43,** 773-781.

[42] Y. H. F. Al-qudah, G. A. Mahmoud and M. A. Abdel Khalek, *J. Radiat. Res. Appl. Sci*., 2014, **7,** 135 -145.

[43] G. Wanga, J. Liu, X. Wang, Z. Xie and N. Deng, *J. Hazard. Mater.*, 2009, **168,** 1053-1058.

[44] P. Ilaiyaraja, Ashish Kumar Singh Deba, K. Sivasubramaniana, D. Ponrajub and B. Venkatramana, *J. Hazard. Mater.,* 2013, **250-251,** 155-166.

[45] S. Yang, J. Li, D. Shao, J. Hu and X. Wang, *J. Hazard. Mater.*, 2009, **166**, 109-116.

[46] G. Bayramoglu, B. Altintas and M. Y. Arica, *Chem. Eng. J.*, 2009, **152,** 339-346.

[47] I. Langmuir, *J. Am. Chem. Soc.,* 1918, **40,** 1361-1368.

[48] H. Freundlich, *Z. Phys. Chem.,* 1906, **57,** 384-470.

[49] G. D. Sheng, L. Ye, Y. M. Li, H. P. Dong, H. Li, X. Gao, and Y. Y. Huang, *Chem. Eng. J.,* 2014, **248**, 71-78.

[50] E. O. Akperov, A. M. Maharramov and O. G. Akperov, *Hydrometallurgy,* 2009, **100,** 76-81.

[51] C. Chen, X. Li, D. Zhao, X. Tan and X. Wang, *Colloids Surf. A Physicochem. Eng. Asp.* 2007, **302**, 449-454.

[52] Ref, Linda Vaisman H. D. Wagner and Gad Marom, *Adv. Colloid Interface Sci.*, 2006, **128-130**, 37-46.

[53] S. Chen, J. Hong, H. Yang and J. Yang, *J. Environ. Radioact.*, 2013, **126,** 253-258.

Figures captions

Fig. 1. IR spectra of CNTs, PVA/E, PVA/ CNTs/E and PVA/ CNTs/SDS/ E hydrogel samples.

Fig. 2. XRD spectra of CNTs, PVA/E, PVA/ CNTs/E and PVA/ CNTs/SDS/ E hydrogel samples

Fig. 3. The degree of swelling (D.S) of PVA/E, PVA/CNTs/E and PVA/CNTs/SDS/ E hydrogel samples of pH 3 at time intervals.

Fig. 4. Scanning electron micrographs of: PVA/E, PVA/CNTs/E, PVA/CNTs/SDS/E, hydrogel samples before and after adsorption of UO_2 ions.

Fig. 5. TEM micrographs of the sample of MWCNTs.

Fig. 6. Effect of pH on the adsorption of uranium.

Fig. 7. Effect of contact time on the adsorption of uranium.

Fig. 8. Effect of initial concentration on the adsorption of uranium

Fig. 9. Langmuir (A) and Freundlich (B) isotherm plots for the adsorption of uranium.

Fig. 10. Plot of $\ln K_d$ versus 1/T for the adsorption of uranium.

Fig. 11. Desorption efficiency of UO_2^{+2} ions from the prepared nanocomposite.

Table 1

Langmuir and Freundlich parameters for uranium (VI) ions adsorption

Composite	Langmuir model			Freundlich model		
	b (L/mg)	Q (mg/g)	R^2	K_F	1/n	R^2
PVA/E	0.0055	121.9512	0.9928	2.7714	1.3383	0.9318
PVA/CNTs/E	0.0029	172.4137	0.9933	3.1470	1.5264	0.9890
PVA/CNTs/SDS/E	0.0024	232.5581	0.9935	3.4127	1.5278	0.9950

Table 2

The thermodynamic parameters for uranium (VI) ions adsorption

Composite	ΔH° (kJ/mol)	ΔS° (J/mol K)	ΔG° (kJ/mol)		
PVA/E	-13.52	6.50	-11.58	-11.43	-11.46
PVA/CNTs/E	-23.79	37.09	-12.49	-12.31	-11.74
PVA/CNTs/SDS/E	-17.26	13.80	-13.03	-13.05	-12.75

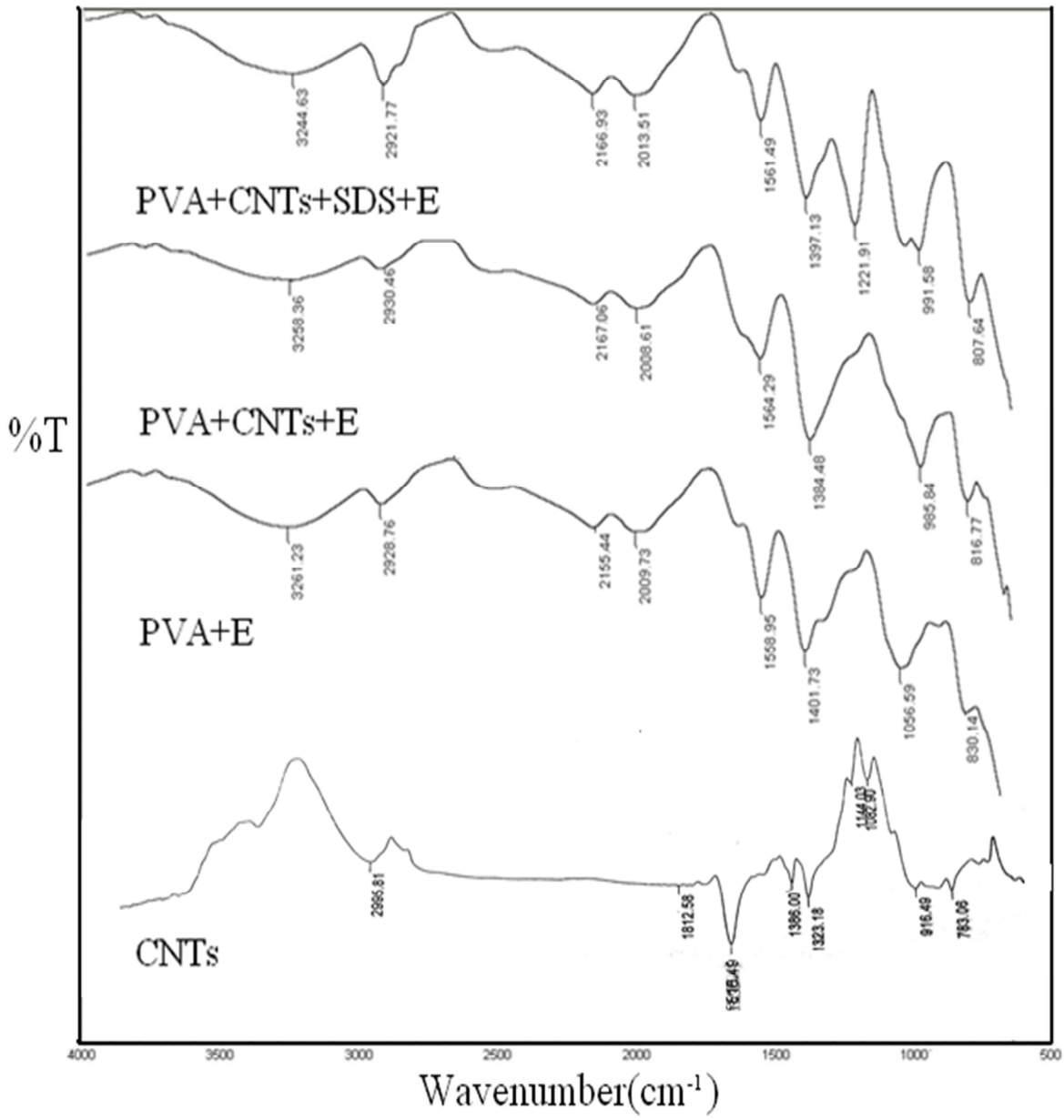

Fig. 1

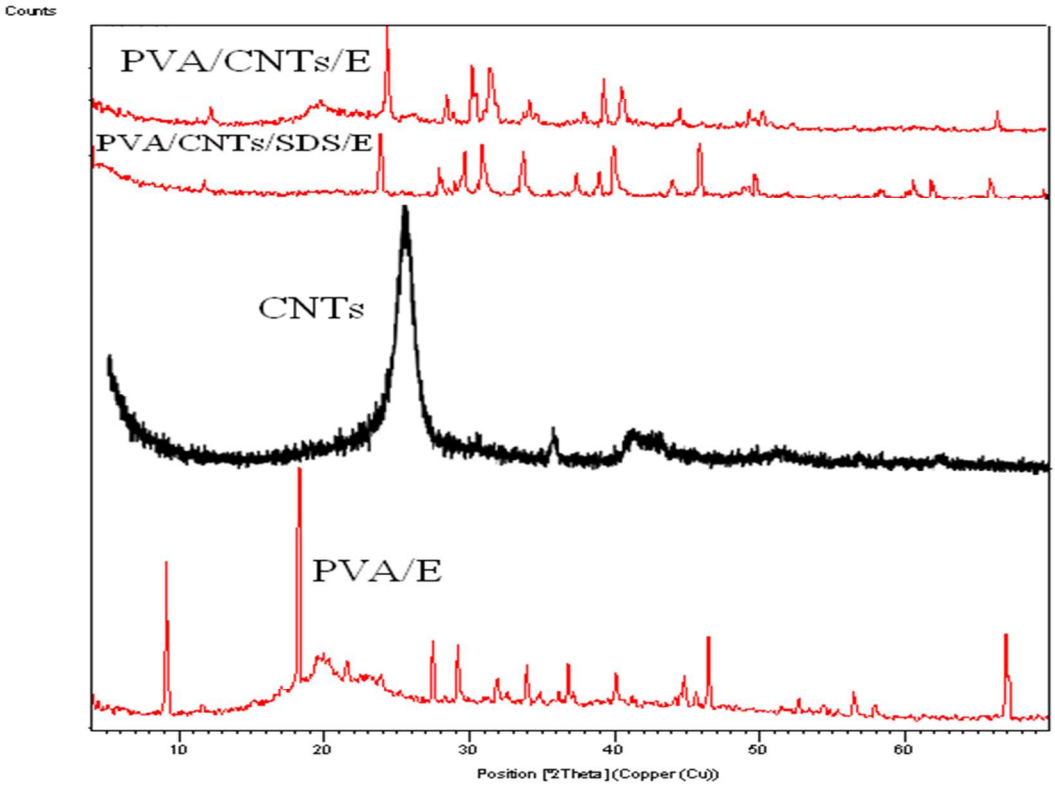

Fig. 2

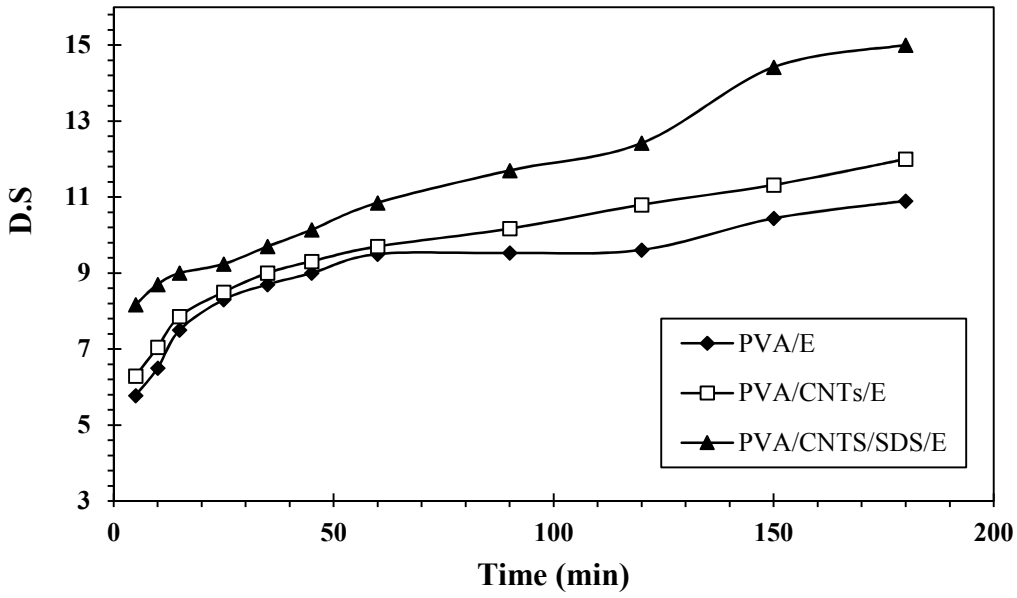

Fig.3

PVA/E

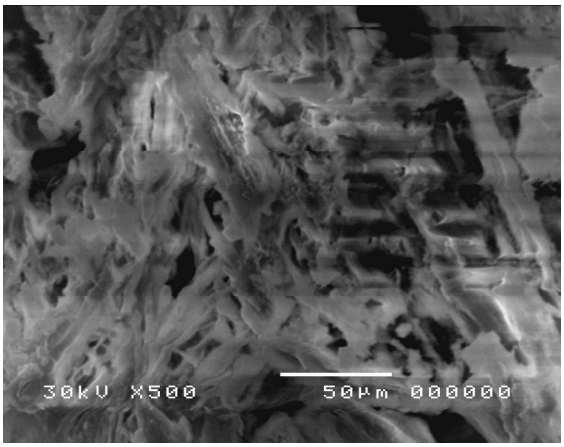

Before adsorption

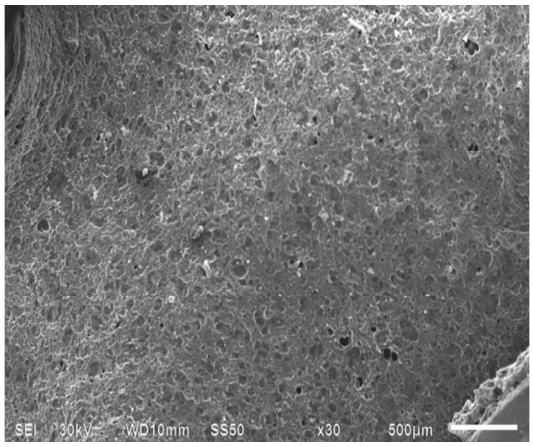

After adsorption

PVA/CNTs/E

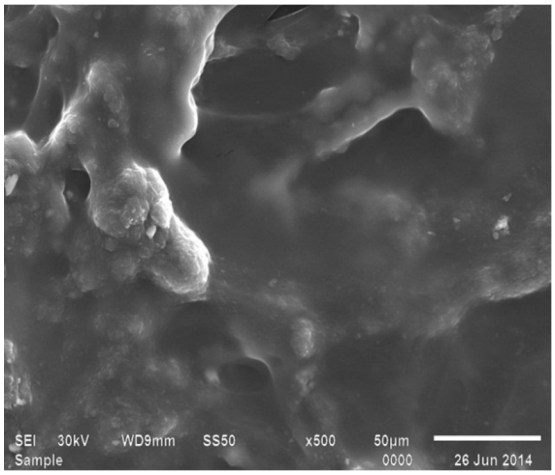

Before adsorption

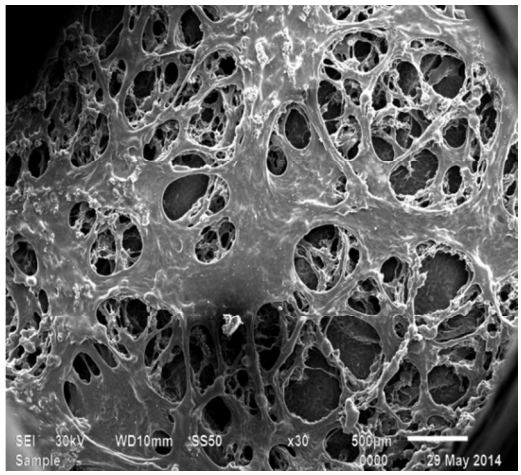

After adsorption

PVA/CNTs/SDS/E

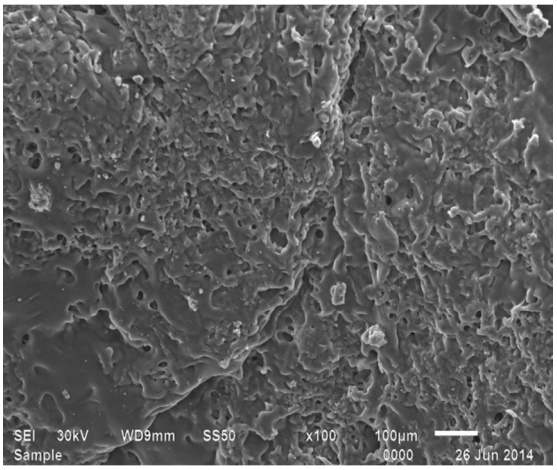

Before adsorption

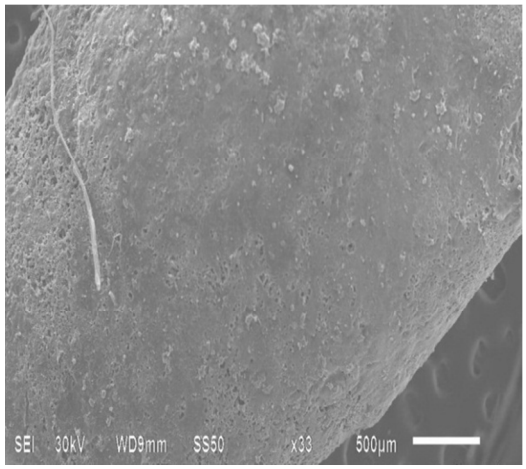

After adsorption

Fig. 4

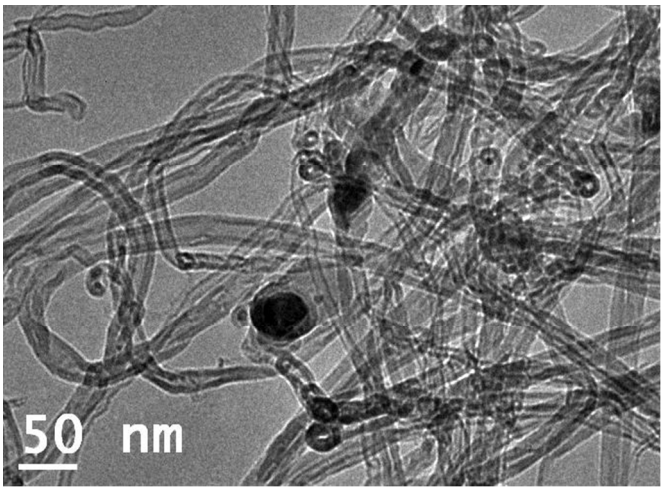

Fig.5

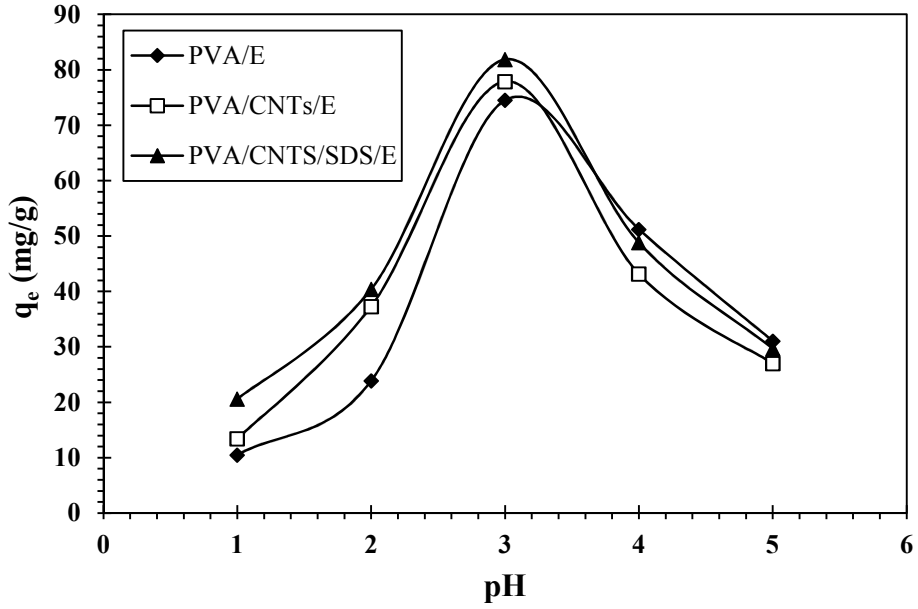

Fig. 6

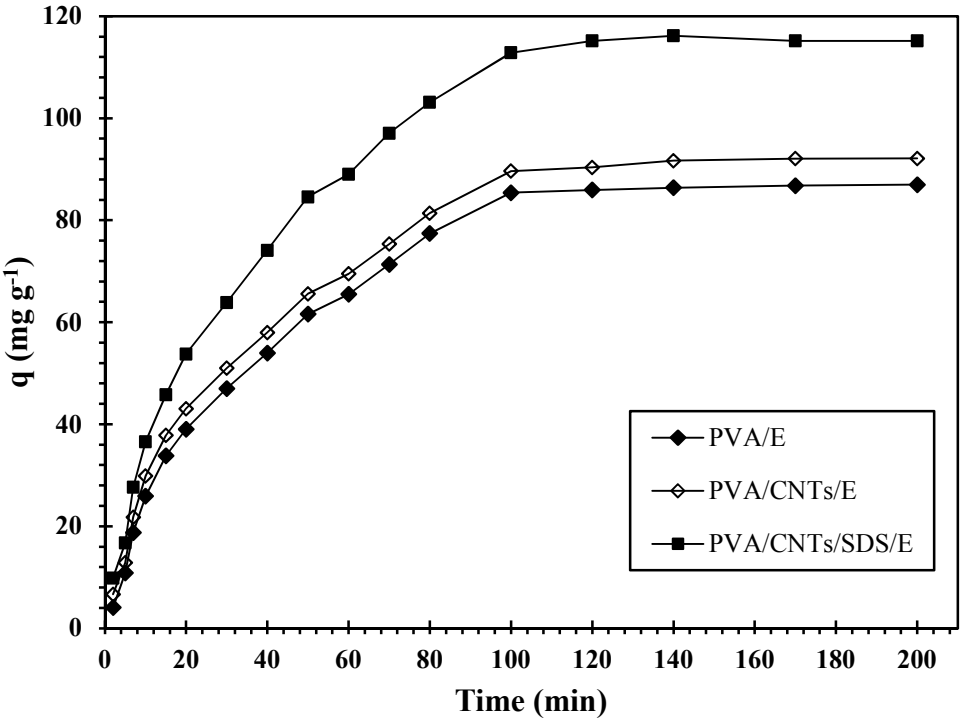

Fig. 7

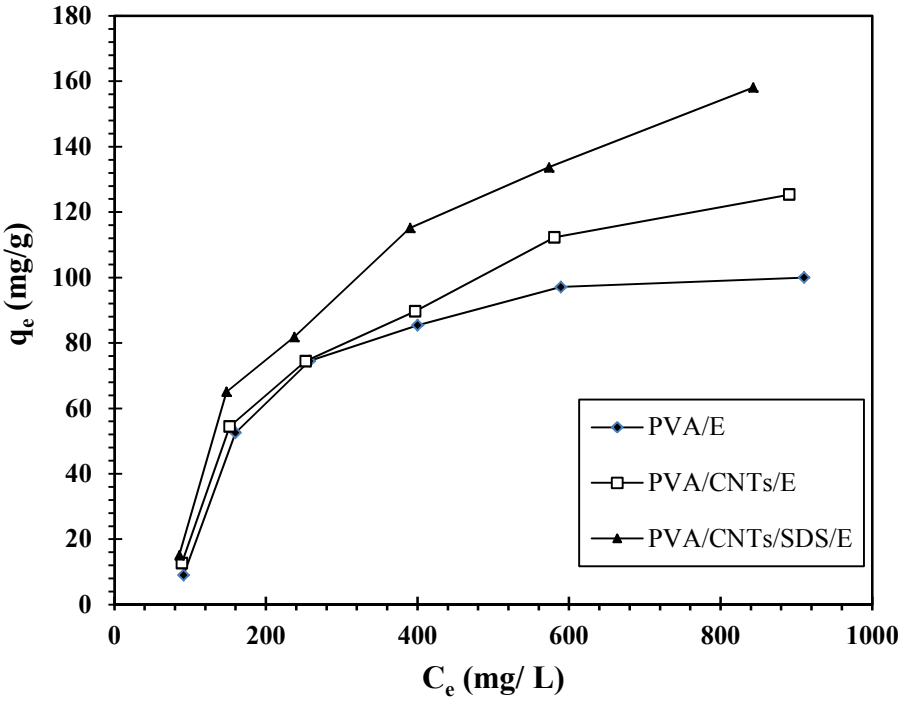

Fig. 8

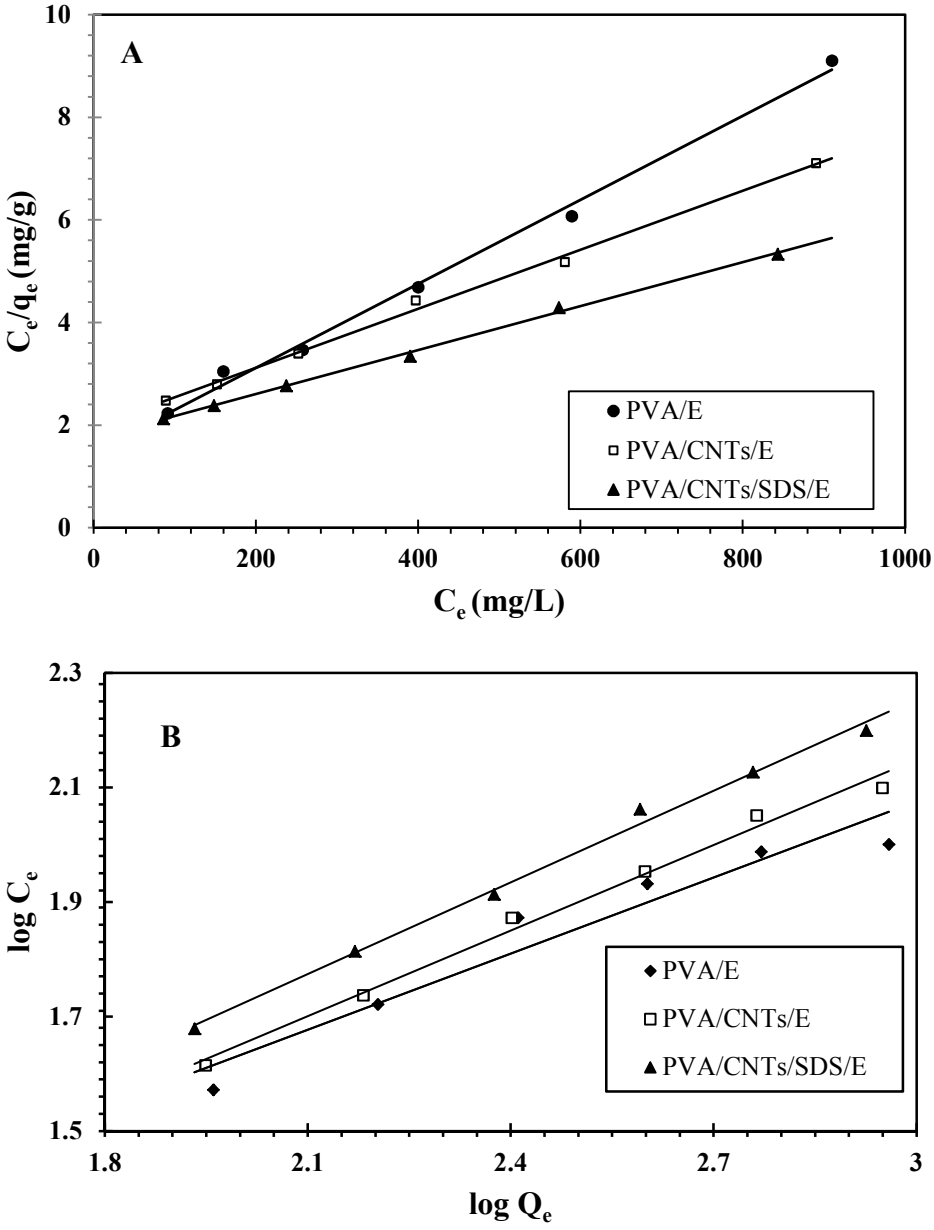

Fig. 9

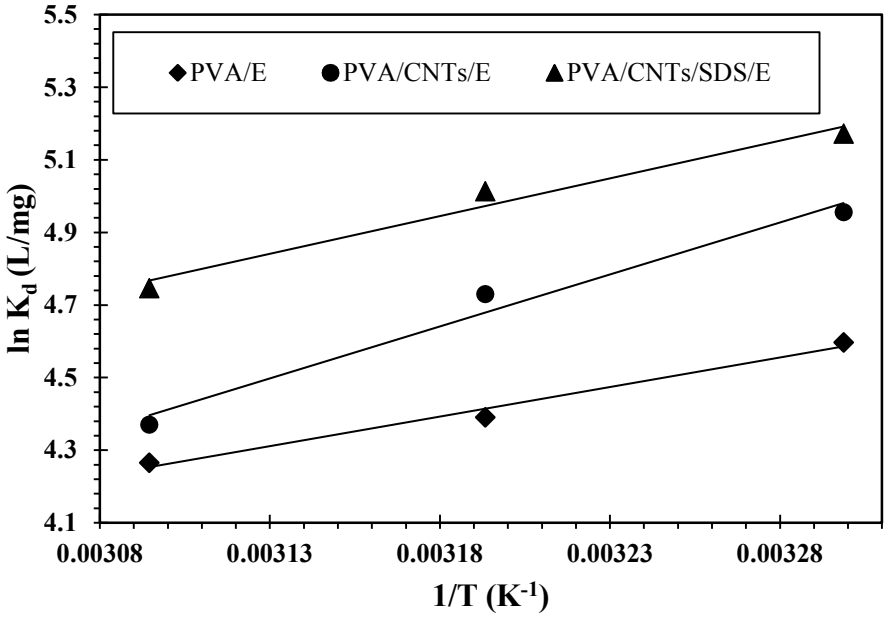

Fig. 10

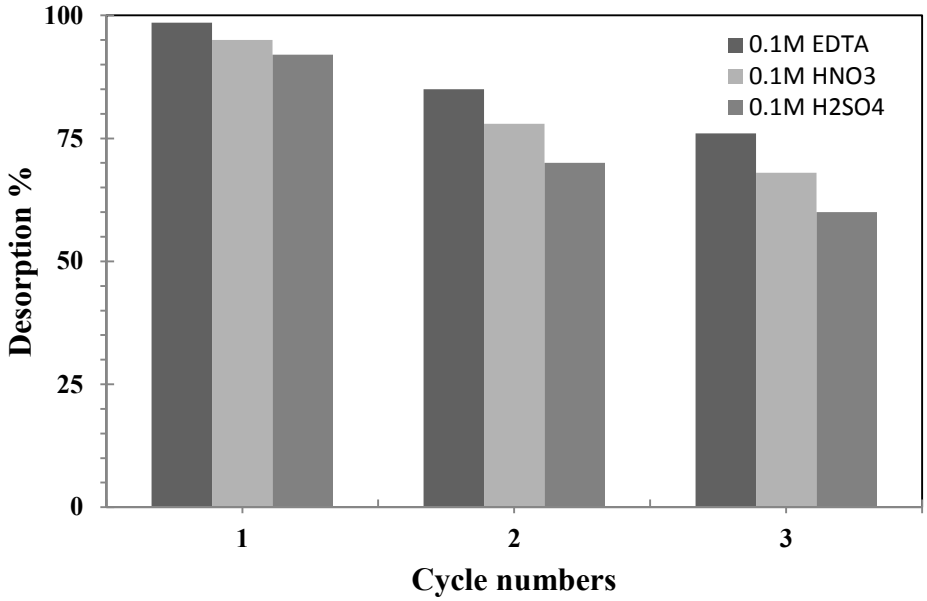

Fig. 11